Demagnetization of electrons in the electromagnetic field structure, typical for quasi-perpendicular collisionless shock front

M. Gedalin and K. Gedalin

Department of Physics, Ben-Gurion University, Beer-Sheva, Israel

M. Balikhin and V. Krasnosselskikh

Laboratoire de Physique et Chimie de l'Environnement, CNRS, Orleans, France

1. 1. Introduction

It is widely believed that electrons in quasi-perpendicular collisionless shocks are heated primarily due to the presence of a quasi-stationary electric field in the shock front [*Goodrich and Scudder,* 1984; *Feldman,* 1985; *Scudder et al.,* 1986b,c; *Schwartz et al.,* 1988; *Veltri et al.,* 1990].

The electrons are traditionally believed to be strongly magnetized in the shock, since even in its narrowest part (ramp) the shock is much wider than the electron gyroradius $\rho_e = v_\perp/\Omega_e$. It is found that the width of the ramp of a subcritical shock is $(1 \div 2)L_W$, where $L_W = 2\pi \cos/(M^2-1)^{1/2}\omega_{pi}$ is the whistler precursor wavelength [*Mellott and Greenstadt*, 1984; *Farris et al.*, 1993], even when such a precursor does not exist. (Here θ is the angle between the upstream magnetic field and the shock normal, M is the upstream Alfven Mach number, and ω_{pi} is the ion plasma frequency.)

In the only published analysis of a supercritical shock front [*Scudder et al.,* 1986a,b,c] the ramp width was found to be in the range $(0.3-1.5)L_W$. Although at present there is no theory that could convincingly explain why the ramp width should be of the order of L_W (the phase-standing whistler precursor cannot exist at high Mach number shocks with $M \geq 5$, see, for example, *Kennel et al.* [1985]) we will adopt this as an empirical fact.

The ratio of the ramp width to the electron gyroradius is then $\sim L_W/\rho_e \sim (m_i/m_e)(\pi\cos\theta/M)(v_A/v_\perp) \gg 1$, unless $v_\perp$ is very high, or $M \sim (m_i/m_e)^{1/2} = 42$.

The scale of the electric field inside the shock front is less certain. The $3\,s$ average data presented by *Scudder et al.* [1986a] do not allow to resolve the ramp scale. On the other hand, *Heppner et al.* [1978] report the presence of DC electric fields with the scales of c/ω_{pe}. These observations are confirmed by *Wygant et al.* [1987] for subcritical shocks. Electron heating observations [*Montgomery et al.*, 1970] (see also *Feldman* [1985, and references therein]), which show that the heating occurs at extremely small scales or at least at the very upstream edge of the shock front, also indirectly confirm the conclusion that the electric field scales are rather small and apparently not larger than the ramp width itself. There is no indication, however, that this scale becomes less than the electron gyroradius. In the present paper we assume that the electric field scale is of the order of the ramp width and analyze the dependence of the electron motion features on the ramp width.

The above mentioned magnetization of electrons implies that the ratio $v_\perp^2/B$ is conserved throughout the shock (subscripts $\parallel$ and $\perp$ refer to the local magnetic field direction). For an initially magnetized electron which proceeds toward downstream across the ramp, the magnetization can only become stronger, since $\rho_e \propto v_\perp/B \propto B^{-1/2}$, while B increases.

If this adiabatic scenario is correct, the only way by which an electron can get perpendicular energy while crossing the ramp is the magnetic moment conservation, while most of the cross-shock electric potential energy is transferred to the parallel degree of freedom. The only way to increase the perpendicular energization is to break the adiabaticity.

There are several reasons why adiabaticity could be broken. The most obvious is that the ramp width can become comparable to the electron gyroradius. This happens in extremely high Mach number perpendicular shocks, as was shown numerically [*Tokar et al.*, 1986] and also analytically and in data analysis [*Galeev et al.*, 1988a]. In these shocks the ramp can become very narrow, so that $D \sim \rho_e$. The electrons become demagnetized. Strong nonadiabatic electron heating, somewhat similar to ion heating, is typical for these shocks. It should be mentioned that the idea of of particle acceleration due to the breakdown of adiabaticity is well-known in magnetospheric physics (see, for example, *Büchner and Zeleny* [1986]; *Chen and Palmadesso* [1986]).

It was shown [*Galeev et al.*, 1988b] that the shock width may decrease down to scales of the order of the electron gyroradius even in the case of moderate Mach number shocks with $\beta = 8\pi T/B^2 \sim 1$. It was proposed that the ramp width can become of the order of $\sim c/\omega_{pe} \sim \rho_e$ and the electron motion can become nonadiabatic. Scale decrease can also occur in dynamical (nonstationary) shocks due to overturning [*Krasnosselskikh*, 1985].

In most stationary moderate Mach number shocks, however, the ramp width is still much larger than the electron gyroradius, and at a first glance this enforces adiabaticity. However, there are additional factors that can lead to the adiabaticity breakdown.

The adiabaticity condition requires not only that the typical scales should be large but also that the parallel electric field should be weak [*Northrop*, 1963]. This condition can be easily violated in the ramp.

Adiabaticity can be broken by an inhomogeneous $\mathbf{E} \perp \mathbf{B}$. It was first shown by *Cole* [1976] for the case of strictly perpendicular geometry and $\mathbf{B} = const$ that electrons can become demagnetized even if the typical spatial scale is considerably larger than the electron gyroradius. The analysis was extended onto the case of inhomogeneous $\mathbf{B}$ and applied to the problem of electron heating in perpendicular geometry [*Balikhin et al.*, 1989, 1993; *Balikhin and Gedalin*, 1994; *Gedalin et al.*, 1995].

The adiabaticity condition is therefore rather sensitive to the shock scale. Correspondingly, the electron energization features should be also sensitive to the shock width and quite different for wide and narrow shocks.

In the present paper we study the electron motion and energization in the model of electromagnetic fields which resembles the structure of the shock. The main objective is to analyze the dependence of the perpendicular energization on the shock width. Particular attention is devoted to the case where the adiabaticity is broken and the electrons become demagnetized.

The paper is organized as follows. In section 2 we review briefly the difference between the normal incidence frame (NIF) and de Hoffman-Teller frame (HTF). In section 3 we describe analytically the mechanism of the transition to the nonadiabatic motion. The results of the numerical study of the electron motion in the model ramp structure are given in section 4. In section 5 we discuss possible implications for the electron heating problem.

2. 2. NIF and HTF

Both the normal incidence frame and the de Hoffman-Teller frame are applied to consideration of one-dimensional stationary oblique shocks. The importance of the difference between the two frames and the role of the noncoplanar magnetic field were emphasized by *Goodrich and Scudder* [1984].

In the spirit of *Goodrich and Scudder* [1984] and *Scudder et al.* [1986a] we assume that: the shock is one-dimensional; the shock is stationary; and the ramp width is between the ion and electron typical scales.

Let us choose the shock normal along the x axis, and let the coplanarity plane be the xz plane. The NIF is defined by the condition that the upstream fluid velocity is along the shock normal only; that is, $\mathbf{V}_u = (V_u, 0, 0)$. Let us choose the upstream (constant) magnetic field in the form $\mathbf{B}_u = B_u(\cos\theta, 0, \sin\theta)$, where θ is the angle between the upstream magnetic field and the shock normal. The electromagnetic structure of the shock front can be described as follows: $\mathbf{B} = (B_u\cos\theta, B_y(x), B_z(x)), \mathbf{E} = (E_x(x), E_y = V_u B_u \sin\theta/c = \text{const}, 0)$, which follows directly from the Maxwell equations. For simplicity in what follows we assume that $E_x \neq 0$ and $B_y \neq 0$ only inside the ramp $-D < x < D$. The main magnetic field component B_z is also assumed to vary inside this region only. In such a case we refer to the region $x < -D$ as upstream and $x > D$ as downstream. Downstream fluid velocity is not along the normal but has a nonzero V_z component. When introducing the electric potential $\varphi = -\int E_x dx - E_y y$ and vector potential $A_y = \int B_z dx$ and $A_z = -\int B_y dx + B_u \cos\theta y$, one can easily see that the energy $\epsilon = m\mathbf{v}^2/2 + q\varphi$ and generalized momentum $p_z = mv_z + qA_z/c$ are conserved.

The HTF is defined by the condition that the upstream fluid velocity is along the upstream magnetic field (Rankine-Hugoniot relations imply that in this case the downstream fluid velocity is in turn parallel to the downstream magnetic field). This condition implies that the HTF moves relatively to the NIF in the z direction with the shift velocity $V_{sh} = -V_u \tan\theta$. The (nonrelativistic) transformation of the fields between the two frames gives [*Goodrich and Scudder*, 1984]

$$E_y^{HT} = 0, \quad E_x^{HT} = E_x^N + (V_u \tan\theta/c)B_y \tag{1}$$

while $\mathbf{B}$ does not change.

In the oblique shock front, in general, $E_x < 0$ in both frames and $B_y > 0$. One can see that it results in a substantial reduction of the HTF cross-shock potential with respect to the NIF cross-shock potential:

$$\varphi^{HT} = \varphi^N - (V_u \tan\theta/c)\int_{-D}^{D} B_y dx \tag{2}$$

Energy conservation is especially convenient in the HTF, since $\varphi = \varphi(x)$ only, and each electron crossing the shock front gains the same energy in the HTF, namely, $e\varphi^{HT}$.

3. 3. Breakdown of Adiabaticity and Electron Energization

We consider the electron motion in the prescribed electromagnetic fields of the stationary one-dimensional shock. The equations of motion in arbitrary frame (NIF or HTF or any intermediate, moving along z axis with constant velocity with respect to both these frames) read

$$\dot{\mathbf{v}} = -\frac{e}{m}\mathbf{E} - \frac{e}{mc}\mathbf{v}\times\mathbf{B}, \qquad \dot{\mathbf{r}} = \mathbf{v} \tag{3}$$

where $E_y = const$, $B_x = const$, $E_z = 0$, and E_x, B_y and B_z are functions of x only.

Local trajectory stability analysis shows how two initially close trajectories $(\mathbf{r}, \mathbf{v})(t)$ and $(\mathbf{r} + \delta\mathbf{r}, \mathbf{v} + \delta\mathbf{v})(t)$ behave [*Tabor* , 1989]. Linearizing (3) near the trajectory $(\mathbf{r}, \mathbf{v})(t)$, one has in our case

$$\dot{\delta\mathbf{v}} = -\frac{e}{m}\frac{d\mathbf{E}}{dx}\delta x - \frac{e}{mc}\delta\mathbf{v}\times\mathbf{B} - \frac{e}{mc}\mathbf{v}\times\frac{d\mathbf{B}}{dx}\delta x, \quad \dot{\delta\mathbf{r}} = \delta\mathbf{v} \tag{4}$$

Applying usual methods of nonlinear dynamics theory [*Tabor* , 1989], we let $\delta\mathbf{r}, \delta\mathbf{v} \propto \exp(\lambda t)$ and immediately obtain

$$\begin{aligned}&\lambda^4 + \lambda^2(\frac{e}{m}\frac{dE_x}{dx} + \Omega^2 + v_y\frac{d\Omega_z}{dx} - v_z\frac{d\Omega_y}{dx})\\ &+\lambda v_x\frac{d}{dx}\frac{\Omega^2}{2} + [\frac{e}{m}\frac{dE_x}{dx}\Omega_x^2 + v_y\Omega_x(\Omega_z\frac{d\Omega_y}{dx}\\ &-\Omega_y\frac{d\Omega_z}{dx}) + \Omega_x^2(v_y\frac{d\Omega_z}{dx} - v_z\frac{d\Omega_y}{dx})] = 0\end{aligned} \tag{5}$$

where $\Omega_i = eB_i/mc$, $\Omega^2 = \sum_i \Omega_i^2$, and $i = x, y, z$.

If (5) has a root λ with $\Re(\lambda) > 0$, the trajectory is unstable. It is clear that the instability condition depends on the trajectory itself. In the HTF, $v_x = V_u + u_x$, $v_y = u_y$, and $v_z = V_u\tan\theta + u_y$, where V_u, and $V_u\tan\theta$ are the x and z components of the upstream plasma velocity in the HTF, while u_x, u_y, and u_z are deviations of the specific electron velocity from the fluid (average) values, i.e., thermal velocities, so that $u \sim v_T$. To find a condition for the global onset of instability, we make the following assumptions: (1) the electrons are subsonic in the HTF; that is, $v_T \lesssim V_u\cos\theta$, and (2) the electrons are not accelerated yet; that is, we are interested in the onset of instability at the upstream edge of the ramp. In this case we can neglect the terms containing $v(d\Omega/dx)$ in comparison with Ω^2 and one has the following approximate equation for λ:

$$\lambda^4 + \lambda^2(\frac{e}{m}\frac{d}{dx}E_x^N + \Omega^2) + \frac{e}{m}\frac{d}{dx}E_x^N\Omega_x^2 = 0 \tag{6}$$

where the transformation rule (1) is taken into account. It should be noted that (6) is exact when the magnetic field is constant.

The solution of (6) is

$$\lambda_\pm^2 = \frac{\Omega}{2}[\alpha - 1 \pm \sqrt{(\alpha-1)^2 + 4\alpha\cos^2\theta}] \tag{7}$$

and it is clear that the global trajectory instability occurs when

$$\alpha \equiv -\frac{e}{m\Omega^2}\frac{d}{dx}E_x^N > 0 \tag{8}$$

This analysis shows that if the electric field slope becomes large, the electron trajectories begin to diverge. We will analyze the trajectories themselves in the limits $|\alpha| \ll 1$ and $|\alpha| \gg 1$, assuming that the typical scale of the inhomogeneity $\gg \rho_e$.

If $|\alpha| \ll 1$, we may neglect the variation of the electric field. The solution is known: $\mathbf{E}\times\mathbf{B}$ drift + gradient drift + gyration. The gradient drift produces the adiabatic perpendicular energization $v_\perp^2 \propto B$.

In the case $|\alpha| \gg 1$ we Taylor expand $E_x^N = E_0^N + (dE_x^N/dx)\cdot x$ and assume $dE_x^N/dx \approx const$. Without loss of generality we put $E_0^N = 0$. For electrons with the initial velocity $\mathbf{V} \approx (V_u, 0, 0)$ in the NIF we may neglect the influence of the magnetic field and obtain approximately $\ddot{x} = \alpha\Omega x$ which gives trapping

$$x \approx -\frac{V}{\Omega\sqrt{|\alpha|}}\sin(\sqrt{|\alpha|}\Omega t), \quad v_x \approx V\cos(\sqrt{|\alpha|}\Omega t) \tag{9}$$

for $\alpha < 0$ and $|\alpha| \gg 1$, and exponential electron runaway along the shock normal

$$x \approx \frac{V}{2\sqrt{\alpha}\Omega}\exp(\sqrt{\alpha}\Omega t), \quad v_x \approx \sqrt{\alpha}\Omega x \tag{10}$$

for $\alpha \gg 1 > 0$.

The most prominent effect is the drastic increase of the v_x component. For a particle, entering the region along the magnetic field line, almost all the potential energy goes into the x directed motion energy; therefore at least the fraction $\sin\theta$ of the electric potential energy goes into the particle gyration energy, in a drastic contrast with what happens in the adiabatic case. Electrons are effectively demagnetized by the large gradient electric field.

It should be emphasized that this breakdown of adiabaticity occurs for particles with small gyroradii $(\rho_e/\Omega)\,(d\Omega/dx) \ll 1$. According to the naive point of view in this case the motion should be adiabatic. It is the presence of the inhomogeneous $\mathbf{E}\perp\mathbf{B}$ that causes the described nonadiabaticity [*Cole*, 1976; *Balikhin et al.*, 1993].

Taking into account all of the above, the global strong nonadiabaticity condition can be written in the following form:

$$\frac{e}{m\Omega^2}|\frac{dE_x}{dx}| \gtrsim 1, \tag{11}$$

where $\Omega = \Omega(x)$ is the local gyrofrequency.

In a real shock ramp the coplanar magnetic field B_z (main component) is not constant, and there is a fairly large component of the noncoplanar magnetic field B_y. The role of $B_z(x)$ is to decrease the corresponding α by increasing the local gyrofrequency Ω in the denominator of (8), thus reducing also the region where the global nonadiabaticity condition holds. Therefore only a part of the cross-shock potential energy can be transferred into the particle gyration energy.

The role of the noncoplanar magnetic field $B_y(x)$ is more complicated. It helps $B_z(x)$ to restore the adiabaticity, since $\Omega = (e/mc)(B_x^2 + B_y^2 + B_z^2)^{1/2}$. It also plays a significant role in the (possible) reflection of electrons with large initial $v_\perp^2$. It also affects greatly the electron motion in the case of large initial $v_\perp$ (see (13)). Last but not least, it reduces the HTF cross-shock potential as compared to the NIF potential.

Nevertheless, the arguments above can be applied to the realistic case as well, if the condition (11) holds, since in the strongly nonadiabatic case, as we have seen before, the particles become effectively demagnetized and almost do not feel the magnetic field (in a part of the ramp). The influence of the magnetic field becomes significant, when $(V/B_y)(dB_y/dx)$ $\sim (V/\Omega L) \sim 1$, where V is the accelerated particle velocity and L is the typical scale of the B_y gradient.

Summarizing all said above, let us qualitatively describe what happens with an electron entering the ramp with initial parallel velocity $v_{u\|}$ and gyration velocity $v_{u\perp}$:

1. The adiabatic scenario is that the gyration energy is proportional to the total magnetic field, so that after crossing the ramp the gyration energy is $v_{d\perp}^2 = v_{u\perp}^2(B_d/B_u)$. The parallel velocity can be found from the energy conservation: $v_{d\|}^2 = v_{u\|}^2 + 2e\varphi^{HT}/m - v_{u\perp}^2((B_d/B_u) - 1)$. 2. For the nonadiabatic scenario, let the adiabaticity be strongly broken in the region $x < x_c$. Then at the point x_c the gyration energy is approximately $v_{c\perp}^2 = v_{u\perp}^2 + 2e\varphi(x_c)/m$. When the particle crosses over the critical point $x = x_c$, adiabaticity is restored, and the gyration energy, as above, is $\propto B$, so that $v_{d\perp}^2 = (v_{u\perp}^2 + 2e\varphi(x_c)/m)(B_d/B(x_c)$ while the parallel energy again is determined by the energy conservation. This simple description can be violated by large initial $v_{u\perp}$. In this case the initial phase dependence becomes very strong, and it can even happen that downstream $v_{d\perp} < v_{u\perp}$ (see numerical analysis below).

It should be emphasized once again that in this case the adiabaticity is broken, although the typical spatial scale is considerably larger than the particle gyroradius. The breakdown of adiabaticity is strong for all electrons in the body of the distribution [cf. *Cole*, 1976; *Balikhin et al.*, 1993]. It becomes weaker for the tail of the electron distribution.

4. 4. Numerical Analysis

Although we succeeded in describing qualitatively the electron motion in the shock ramp in both adiabatic and nonadiabatic cases, it still does not seem possible to perform a quantitative analysis analytically. Instead, we study numerically electron trajectories in the model ramp structure, tracing electron trajectories in the prescribed stationary electromagnetic fields. No back influence of the electrons onto the field structure is taken into account.

The problem is essentially dimensionless; that is, while the absolute values of the input and output parameters may vary in a wide range, the relative values (as, for example, fraction of the initial ion energy that goes into the perpendicular energization) depend on a set of dimensionless initial shock parameters. The set of the shock parameters that are measured experimentally and are input parameters for the numerical model looks as follows: the upstream Alfven Mach number M; the ratio $B_{zd}/B_{zu} = r$; and the angle between the shock normal and upstream magnetic field θ. This is completed with the electric field and scale parameters (which are not measured with confidence so far): the relative NIF potential drop $s_1 = e\varphi^N/\epsilon_i$, where $\epsilon_i = m_i V_u^2/2$ is the upstream NIF ion energy; the relative HTF potential drop $s = e\varphi^{HT}/\epsilon_i$; the ramp half width D measured in the whistler half-lengths $l_W = \pi c \cos\theta/M\omega_{pi}$ (we assume that the fields change only inside $-Dl_W < x < Dl_W$ region).

The model B_z profile is chosen as a simplest polynomial which is continuous with its first and second derivatives at $x = \pm Dl_W$ and does not vary outside the ramp:

$$B_z = B_u \sin\theta\left(\frac{r+1}{2} + \frac{r-1}{16}(3\zeta^5 - 10\zeta^3 + 15\zeta)\right), \tag{12}$$

where $\zeta = x/Dl_W$, $r = B_{zd}/B_{zu}$ and B_u is the total upstream magnetic field.

The component B_y is chosen to be the theoretical [*Jones and Ellison*, 1987] $B_y \propto dB_z/dx$ but with a phenomenological coefficient which provides the necessary difference between the NIF and HTF potentials according to (2).

The choice of the profile of the electric field E_x is more complicated. We assume that there is a substantial potential drop applied at the ramp only and that the electric field inside the ramp is not structured with smaller scales present. Both assumptions are definitely not precise and a more detailed form of the cross-shock potential profile should be known before one is going to compare directly the numerical results with observations. Both assumptions are, however, quite suitable for the present study, in which we analyze the results of the adiabaticity breakdown and their dependence on the field parameters, when such a breakdown occurs.

For the present model we combine the theoretical estimate (see, for example, *Gedalin et al.* [1995])

$$eE_x^N \propto -\frac{1}{8\pi n}\frac{d\mathbf{B}^2}{dx}, \quad n \propto B \tag{13}$$

with the phenomenological model requirement $\varphi(Dl_W) - \varphi(-Dl_W) = s_1\epsilon_i$ to obtain

$$e\varphi^N = \frac{s_1\epsilon_i}{B_d - B_u}\frac{dB}{dx}, \tag{14}$$

where $B = (B_x^2 + B_y^2 + B_z^2)^{1/2}$ is the total magnetic field and B_u and $B_d = B_u(\cos^2\theta + r^2\sin^2\theta)^{1/2}$ are the upstream and downstream total magnetic fields, respectively.

It is worth noting that the strong nonadiabaticity condition takes the following approximate form

$$\frac{s_1 M^4}{2D^2\pi^2\cos^2\theta}\frac{m_e}{m_i} \gtrsim 1. \tag{15}$$

We emphasize that the NIF electric field (factor s_1) and not the HTF electric field determines the condition (see sections 2 and 3).

The following parameters are taken as constant throughout the numerical analysis in the present paper: upstream Mach number $M = 6$, angle between the shock normal and upstream magnetic field $\theta = 75\,\mathrm{deg}$, ratio $r = B_{zd}/B_{zu} = 3$. The basic choice of the dimensionless cross-shock potential is $s_1 = 0.6$ (NIF), $s = 0.15$ (HTF), although in several runs these are varied. This choice is consistent with numerical simulations [*Goodrich*, 1985] and observations [*Scudder et al.*, 1986b; *Thomsen et al.*, 1987].

The most important variable parameter is the ramp half width D for which both theory and observations [*Scudder et al.*, 1986a] predict $D \sim 1$. The nonadiabaticity parameter $\alpha = (2/m)|dE_x/dx|/\Omega^2$ (inside the ramp) for several different ramp half widths is shown in Figure 1. Other parameters, specific for each separate run, are given below.

We trace the particle trajectories from far upstream to far downstream, beginning at the point where there was not yet interaction with the ramp fields and finishing at the point where there was not already interaction with the ramp fields. The following output dimensionless parameters characterize the electron energization mode: parallel energization $h_l = \Delta\epsilon_\parallel/e\varphi^{HT}$; fraction of HTF cross-shock potential which goes to the perpendicular energization $h_t = \Delta\epsilon_\perp/e\varphi^{HT}$; perpendicular energization efficiency $h_e = \Delta\epsilon_\perp/\epsilon_i$; and overadiabaticity $h_o = \epsilon_\perp/\epsilon_{ad}$, where $\Delta\epsilon_{\parallel,\perp} = \epsilon_{d\parallel,\perp} - \epsilon_{u\parallel,\perp}$, $\epsilon_{\parallel,\perp} = m_e v_{\parallel,\perp}^2/2$, $\epsilon_i = m_i V_u^2/2$, and $\epsilon_{ad} = \epsilon_{u\perp}(B_d/B_u)$. Obviously, $h_l + h_t = 1$.

In the present numerical analysis the initial conditions read (hereforth we measure lengths in l_W and velocities in V_u, where V_u is the NIF upstream fluid velocity) $v_x = V_l\cos\theta + V_p\cos\phi\,\sin\theta$, $v_y = V_p\sin\phi$, $v_z = V_l\sin\theta - V_p\cos\phi\,\cos\theta$, at $t = 0$. Initial $x = x_0$ is taken always outside the ramp at a distance greater than the electron gyroradius. Initial y and z are arbitrary due to the translational symmetry. The initial phase ϕ is defined at $x = x_0$ and not at the ramp boundary, so that for different D (ramp half width) the electrons enter the ramp with different phases at the ramp boundary.

In Figures 2 and 3 we present the results of trajectory analysis for the case when the initial dimensionless perpendicular velocity $V_p = 0$; that is, when an adiabatic electron would cross the ramp, moving all the time along the magnetic field line. Initial parallel velocity $V_l = 1/\cos\theta = 3.86$; that is, the electron moves with the bulk plasma velocity. Figures 2a and 3a show the x-component of the electron velocity (the most representative, see section 3) as a function of the coordinate x along the shock normal. Figures 2b and 3b show the (dimensionless) fields (inside the ramp only) as functions of x/D: Bt, total magnetic field $b_t(z) = (b_x^2 + b_y^2 + b_z^2)^{1/2}$, By, noncoplanar component of the magnetic field $b_y(z)$, N, NIF cross-shock potential $\varphi^N(x/D)$, and HT, HTF cross-shock potential $\varphi^{HT}(x/D)$.

Figure 2 corresponds to the adiabatic case $D = 3$. One can see from Figure 1 that the corresponding α is small. As could be expected, the electron, which enters the ramp along the field line, proceeds along it and does not gain perpendicular energy. The corresponding perpendicular energization is negligible, $h_t = 0$.

Figure 3 corresponds to the strongly nonadiabatic case $D = 1$. The corresponding α is large, as seen from Figure 1. In contrast with the case shown in Figure 2, the electron, which enters the ramp along the magnetic field line, is efficiently accelerated along the shock normal in the region where $\alpha \gtrsim 1$ and therefore acquires substantial gyration energy. The corresponding perpendicular energization $h_t = 0.75$. A closer inspection of Figures 3 and 1 shows that the region of the acceleration approximately coincides with the region where $\alpha \gtrsim 1$. It should be emphasized that the adiabaticity is broken strongly, although in this case $\rho_e = 0$.

In Figure 4 we present the dependence of the perpendicular energization h_t on the ramp half width D for different values of the dimensionless NIF potential s_1 and constant HTF potential $s = 0.15$. As could be expected, the energization increases with the increase of s_1, since the nonadiabaticity parameter $\alpha \propto s_1$.

In Figure 5 we present the dependence of the perpendicular energization (Figure 5a) and efficiency (Figure 5b) as a function of the ramp half width D for different values of the dimensionless HTF potential s and constant NIF potential $s_1 = 0.6$. The efficiency h_e depends on s only weakly. The decrease of h_t with the increase of s is a consequence of the relation $h_t = h_e/s$.

In Figure 6 we present dependence of the perpendicular energization ((Figure 6a) and overadiabaticity ((Figure 6b) on the initial gyration velocity V_p for the initial phase $\phi = 0$ and different ramp half widths D. One can see almost exactly adiabatic energization in the case of the wide ramp $D = 3$ and irregular energization in the nonadiabatic cases $D = 1$ and $D = 1.2$. In the latter case underadiabatic energization is observed: the electron looses gyration energy. This phenomenon

can be explained as an unfortunate competition between acceleration in the nonadiabatic region and subsequent adiabatic behavior when the adiabaticity is restored. Resulting energization appears to be smaller than the adiabatic one for large initial gyration velocities. One can see also that the nonadiabatic energization in the case $D = 1$ approaches the adiabatic values for large V_p. Similar behavior was observed in the simulations of ion heating [*Lee et al.*, 1986]. The observed irregularities also indicate on rather strong sensitivity on the initial conditions and the details of the field profile.

The phase dependence of the perpendicular energization is shown in Figure 7 for two different initial velocities $V_p = 4$ ((Figure 7a) and $V_p = 2$ ((Figure 7b) and three different D. The upper and lower curves and the straight line correspond to $D = 1$, $D = 1.2$, and $D = 3$, respectively. One can see that the energization is independent of the phase in the adiabatic case, while in the nonadiabatic case the dependence is strong and is stronger for larger V_p and smaller D.

5. 5. Discussion

The analysis above has shown that the electron energization is quite different in wide and narrow shocks. While in the former the electrons are accelerated along the magnetic field, in the latter the electrons gain substantial perpendicular energy directly from the cross-shock potential. What happens in reality depends on the actual shock parameters, particularly on the field profiles in the ramp.

Being optimists we would say that the three-dimensional magnetic field profile $\mathbf{B}(\mathbf{r})$ is measured. However, the shock electric field, which is crucial, remains unknown (either due to the lack of high-resolution measurements or because of the lack of the corresponding data analysis). In the present paper, in order to study single particle effects, we used a model structure.

Nonadiabatic behavior will definitely result in a stronger perpendicular heating than in the adiabatic case. Although single particle studies cannot provide even a rough estimate of this heating, several conclusions can be still derived. First, one can see from Figure 7a that in the nonadiabatic case $D = 1$, electrons acquire $\geq 40\%$ of the cross-shock potential energy independently of the initial phase, which means the energization is not phase selective. Second, from Figure 6 one can conclude that the nonadiabatic energization is large for small V_p, i.e., for the core of the electron distribution and not for the tail (this is an important feature of the presented nonadiabatic energization). As a result most electrons will benefit from the nonadiabatic energization.

To make more quantitative conclusions, a distribution behavior should be analyzed, which is beyond the scope of the present paper.

Such analysis of the distribution behavior for two cases (adiabatic and nonadiabatic) was done recently by *Gedalin et al.* [1995].

6. 6. Conclusions

We have shown in the present paper the following:

1. In a sufficiently narrow quasi-perpendicular collisionless shock ramp (if $\alpha \gtrsim 1$) the electrons become demagnetized.

2. The electron nonadiabaticity results in the transfer of a considerable fraction of the cross-shock potential energy into the downstream electron gyration energy.

3. The electron perpendicular energization can greatly exceed adiabatically produced values.

4. The energization efficiency is lower for large initial perpendicular velocities.

5. The energization efficiency depends significantly on initial phase, and this dependence is stronger for large initial perpendicular velocities and smaller ramp widths.

6. The numerically analyzed model parameters are relevant for observed shocks, within the limits of our present knowledge.

Acknowledgments. M. Gedalin is very grateful to C.T. Russell, S.J. Schwartz, and J.D. Scudder for useful discussions. We are also grateful to both referees for stimulating comments.

The Editor thanks R.J. Strangeway and another referee for their assistance in evaluating this paper.

References

Balikhin, M. and M.Gedalin, Kinematic mechanism of electron heating in shocks: Theory versus observations, *Geophys. Res. Lett., , 21,* 841, 1994.

Balikhin, M.A., M.E. Gedalin, and J.G. Lominadze, A possible mechanism of electron heating in collisionless perpendicular shock front, *Adv. Space Res., 9,* 135, 1989.

Balikhin, M., M. Gedalin, and A. Petrukovich, New mechanism for electron heating in shocks, *Phys. Rev. Lett., , 70,* 1259, 1993.

Büchner, J. and L.M. Zeleny, Deterministic chaos in the dynamics of charged particles near a magnetic field reversal, *Phys. Lett. A, 118,* 395, 1986.

Chen, J. and P.J. Palmadesso, Chaos and nonlinear dynamics of single-particle orbits in a magnetotaillike magnetic field, *J. Geophys. Res., , 91,* 1499, 1986.

Cole, K.D., Effects of crossed magnetic and (spatially dependent) electric fields on charged particle motion, *Planet. Space Sci., 24,* 518, 1976.

Farris, M.H., C.T. Russell, and M.F. Thomsen, Magnetic structure of the low beta, quasi-perpendicular shock, *J. Geophys. Res., , 98,* 15,285, 1993.

Feldman, W.C., Electron velocity distributions near collisionless shocks, in *Collisionless Shocks in the Heliosphere: Reviews of Current Research,* Geophys. Monogr. Ser., vol. 35, edited by R.G. Stone and B.T. Tsurutani, pp. 195-205, AGU, Washington, D.C., 1985.

Galeev, A.A., C.F. Kennel, and V.V. Krasnoselskikh, Quasi-perpendicular collisionless high Mach number shocks, in: *Proceedings of the Joint Varenna-Abastumani International School and Workshop on Plasma Astrophysics, Eur. Space Agency Spec. Publ. ESA SP-285*, vol. I, 173, 1988a.

Galeev, A.A., V.V. Krasnosselskikh, and V.V.Lobzin, Fine structure of the front of a quasi-perpendicular supercritical collisionless shock wave, *Sov. J. Plasma Phys. Engl. Transl., 14,* 697, 1988b.

Gedalin, M., M. Balikhin, and V. Krasnosselskikh, Electron heating in collisionless shocks, *Adv. Space Res., 15,* (8/9) 239, 1995.

Goodrich, C.C., Numerical simulations of quasi-perpendicular collisionless shocks, in *Collisionless Shocks in the Heliosphere: Reviews of Current Research,* Geophys. Monogr. Ser., vol. 35, edited by R.G. Stone and B.T. Tsurutani, pp. 153-168, AGU, Washington, D.C., 1985.

Goodrich, C.C., and J.D. Scudder, The adiabatic energy change of plasma electrons and the frame dependence of the cross shock potential at collisionless magnetosonic shock waves, *J. Geophys. Res., , 89,* 6654, 1984.

Heppner, J.P., N.C. Maynard, and T.L. Aggson, Early results from ISEE-1 electric field measurements, *Sp. Sci. Rev., 22,* 777, 1978.

Jones, F.C. and D.C.Ellison, Noncoplanar magnetic fields, shock potentials, and ion deflection, *J. Geophys. Res., , 92,* 11,205, 1987.

Kennel, C.F., J.P. Edmiston, and T. Hada, A quarter century of collisionless shock research, in *Collisionless Shocks in the Heliosphere: A Tutorial Review*, Geophys. Monogr. Ser., vol. 34, edited by R.G. Stone and B.T. Tsurutani, pp. 1-36, AGU, Washington, D.C., 1985.

Krasnoselskikh, V.V., Nonlinear plasma motions across a magnetic field, *Sov. Phys. JETP Engl. Transl., 62,* 282, 1985.

Lee, L. C., C.S. Wu, and X.W. Hu, Increase of ion kinetic temperature across a collisionless shock, I, A new mechanism, *Geophys. Res. Lett., , 13,* 209, 1986.

Mellott, M. M. and E. W. Greenstadt, The structure of oblique subcritical bow shocks: ISEE 1 and 2 observations, *J. Geophys. Res., , 89,* 2151, 1984.

Montgomery, M.D., J.R. Asbridge, and S.J. Bame, Vela 4 plasma observations near the Earth's bow shock, *J. Geophys. Res., , 75,* 1217, 1970.

Northrop, T., *The Adiabatic Motion of Charged Particles,* John Wiley, New York, 1963.

Schwartz, S.J., M.F. Thomsen, S.J. Bame, and J. Stansbury, Electron heating and the potential jump across fast mode shocks, *J. Geophys. Res., , 93,* 12,923, 1988.

Scudder, J.D., A. Mangeney, C. Lacombe, C.C. Harvey, T.L. Aggson, R.R. Anderson, J.T. Gosling, G. Paschmann, and C.T. Russell, The resolved layer of a collisionless, high β, supercritical, quasi-perpendicular shock wave, 1, Rankine-Hugoniot geometry, currents, and stationarity, *J. Geophys. Res., , 91,* 11,019, 1986a.

Scudder, J.D., A. Mangeney, C. Lacombe, C.C. Harvey, and T.L. Aggson, The resolved layer of a collisionless, high β, supercritical, quasi-perpendicular shock wave, 2, Dissipative fluid electrodynamics, and stationarity, *J. Geophys. Res., , 91,* 11,053, 1986b.

Scudder, J.D., A. Mangeney, C. Lacombe, C.C. Harvey, C.S. Wu, and R.R. Anderson, The resolved layer of a collisionless, high β, supercritical, quasi-perpendicular shock wave, 3, Vlasov electrodynamics, *J. Geophys. Res., , 91,* 11,075, 1986c.

Tabor, M., *Chaos and Integrability in Nonlinear Dynamics,* John Wiley, New York ,1989.

Thomsen, M.F., M.M. Mellott, J.A. Stansbury, S.J. Bame, J.T. Gosling, and C.T. Russell, Strong electron heating at the Earth's bow shock, *J. Geophys. Res., , 92,* 10,119, 1987.

Tokar, R.L., C.H. Aldrich, D.W. Forslund, and K.B. Quest, Nonadiabatic electron heating at high-Mach number perpendicular shocks, *Phys. Rev. Lett., , 56,* 1059, 1986.

Veltri, P., A. Mangeney, and J.D. Scudder, Electron heating in quasi-perpendicular shocks: A Monte-Carlo simulation, *J. Geophys. Res., , 95,* 14,939, 1990.

Wygant, J.R., M. Bensadoun, and F.C. Mozer, Electric field measurements at subcritical, oblique bow shock crossings, *J. Geophys. Res., , 92,* 11109, 1987.

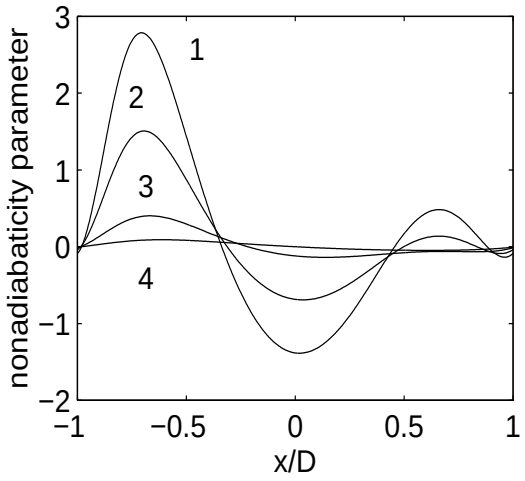

Figure 1. Nonadiabaticity parameter α inside the ramp for different ramp widths $D^{(1)} = 1$, $D^{(2)} = 1.2$, $D^{(3)} = 1.8$, $D^{(4)} = 3$. Other parameters: $s_1 = 0.6$, $s = 0.15$, $R = 3$, and $M = 6$.

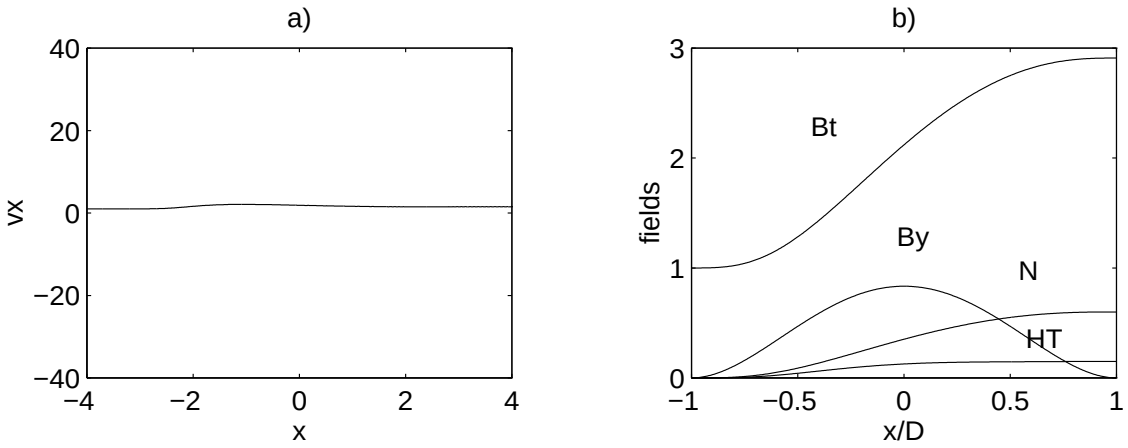

Figure 2. (a) Electron motion (only $v_x(x)$ is shown) and (b) field structure in the adiabatic case $D = 3$. Initial perpendicular velocity $V_p = 0$. Basic parameters: $s_1 = 0.6$, $s = 0.15$, $R = 3$, and $M = 6$. No perpendicular energization $h_t = 0$.

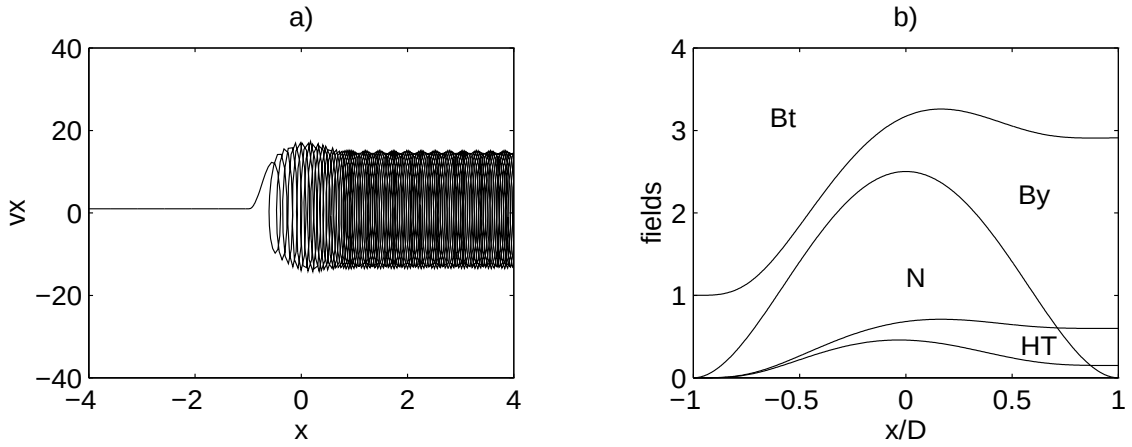

Figure 3. (a) Electron motion (only $v_x(x)$ is shown) and (b) field structure in the nonadiabatic case $D = 1$. Initial perpendicular velocity $V_p = 0$. Basic parameters: $s_1 = 0.6$, $s = 0.15$, $R = 3$, and $M = 6$. Strong perpendicular energization $h_t = 0.75$.

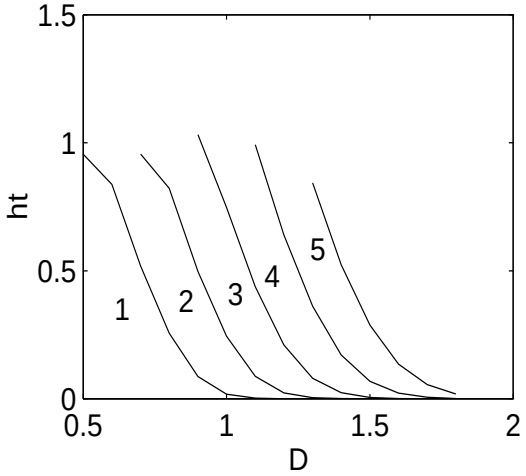

Figure 4. Perpendicular energization h_t as a function of the ramp width D for different values of NIF potential $s_1^{(1)} = 0.4$, $s_1^{(2)} = 0.4$, $s_1^{(3)} = 0.6$, $s_1^{(4)} = 0.7$, $s_1^{(5)} = 0.8$. HTF potential $s = 0.15$.

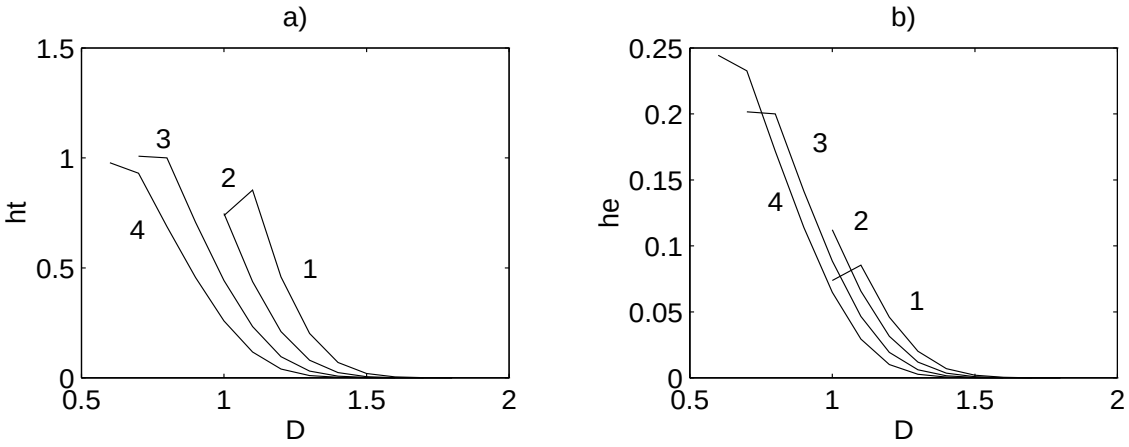

Figure 5. (a) Perpendicular energization h_t and (b) perpendicular efficiency h_e as functions of the ramp width D for different values of HTF potential $s^{(1)} = 0.1$, $s^{(2)} = 0.15$, $s^{(3)} = 0.2$, $s^{(4)} = 0.25$. NIF potential $s_1 = 0.6$.

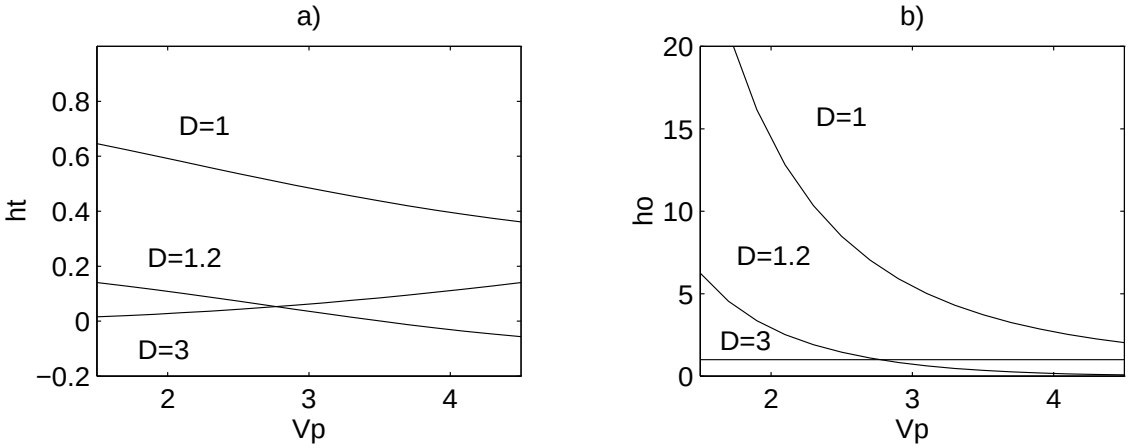

Figure 6. (a) Perpendicular energization h_t and (b) overadiabaticity h_o as functions of the initial perpendicular velocity V_p for the initial phase $\phi = 0$ and different ramp half widths D.

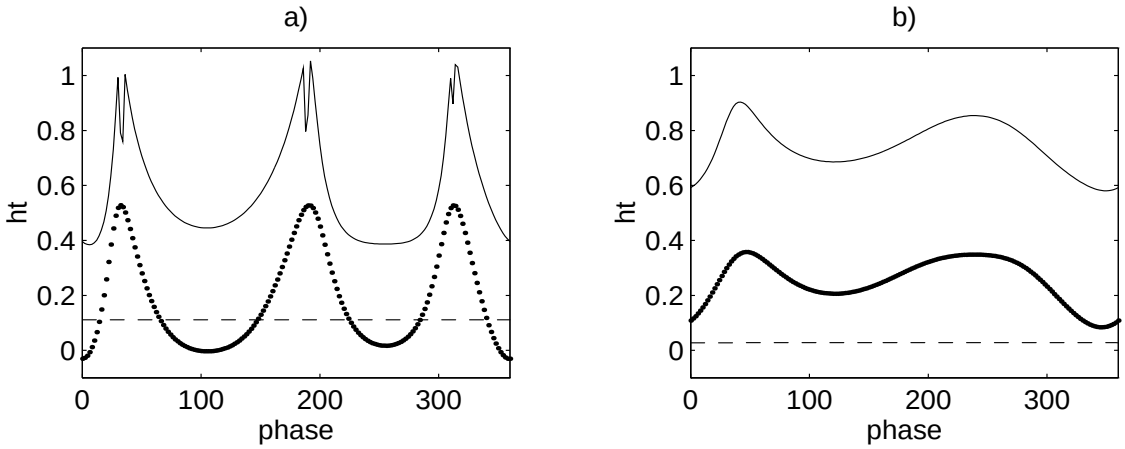

Figure 7. Dependence of the perpendicular energization on the initial phase for the initial perpendicular velocity (a) $V_p = 4$ and (b) $V_p = 2$. Upper and lower curves and straight line correspond to $D = 1$, $D = 1.2$, and $D = 3$, respectively.